RSC Medicinal Chemistry

ROYAL SOCIETY OF CHEMISTRY

RESEARCH ARTICLE

View Article Online
View Journal | View Issue

Cite this: *RSC Med. Chem.*, 2024, **15**, 1216

A novel BODIPY-based theranostic agent for *in vivo* fluorescence imaging of cerebral Aβ and ameliorating Aβ-associated disorders in Alzheimer's disease transgenic mice†

Jingjing Zhang,‡[abc] Wenming Ren,‡[ab] Xiaohui Liu,[ac] Jingjing Chen,[d] Yuteng Zeng,[ae] Huaijiang Xiang,[ac] Youhong Hu*[acd] and Haiyan Zhang *[abc]

Received 27th December 2023,
Accepted 19th February 2024

DOI: 10.1039/d3md00744h

rsc.li/medchem

β-Amyloid (Aβ) aggregation is increasingly recognized as both a biomarker and an inducer of the progression of Alzheimer's disease (AD). Here, we describe a novel fluorescent probe **P14**, developed based on the BODIPY structure, capable of simultaneous visualization and inhibition of Aβ aggregation *in vivo*. **P14** shows high binding affinity to Aβ aggregates and selectively labels Aβ plaques in the brain slices of APP/PS1 mice. Moreover, **P14** is able to visualize overloaded Aβ in both APP/PS1 and 5 × FAD transgenic mice *in vivo*. From the aspect of potential therapeutic effects, **P14** administration inhibits Aβ aggregation and alleviates Aβ-induced neuronal damage *in vitro*, as well as reduces central Aβ deposition and ameliorates cognitive impairment in APP/PS1 transgenic mice *in vivo*. Finally, **P14** is applied to monitor the progression of Aβ aggregation in the brain of 5 × FAD transgenic mice and the intervention effect itself by fluorescence imaging. In summary, the discovery of this fluorescent agent might provide important clues for the future development of theranostic drug candidates targeting Aβ aggregation in AD.

Introduction

Alzheimer's disease (AD) is a prevalent and disabling neurodegenerative disorder accompanied by a series of mental state changes, and eventually leads to dementia.[1] Despite numerous efforts in the development of "disease modifying" treatment, most drug candidates failed to show satisfactory clinical benefits in halting the disease progression of AD patients. One of the restriction factors that hinder the successful development of anti-AD drugs is ineffective identification and validation of key biomarkers for the early diagnosis of AD.[2] According to the AD biomarker model summarized by R. Sperling *et al.*, the appearance of β-amyloid (Aβ) deposition is much earlier than the occurrence of the clinical state of AD.[3] Besides, central Aβ overload causes synaptic damage and consequently induces learning and memory deficits.[4] Therefore, it is a reasonable assumption that Aβ has already caused irreversible nerve damage when clinical symptoms appear, and is recognized as an important biomarker for both diagnosis and treatment of AD.

In recent years, fluorescence imaging has become a powerful and inexpensive tool as a non-invasive imaging method *in vivo*.[5] Many fluorescent probes with various structures have been used to label Aβ aggregates *in vitro*, and several compounds have good capability to label Aβ plaques in the brain of transgenic animals.[6–11] However, current methods for diagnosing and treating disease are separately hampered by their inability to respond locally and dynamically to disease states.[12] The combination of diagnosis and treatment can be a better way to provide real-time knowledge of the internal disease state, contributing to early diagnosis besides providing a holistic transition from "trial and error" concept to "precise, targeted and personalized" concept therapeutics.[13] This led to the development of a remarkable platform known as theranostics.

The concept of theranostics has been widely used in the study of tumors[13] and cardiovascular disease,[14,15] nevertheless,

[a] *State Key Laboratory of Drug Research, Shanghai Institute of Materia Medica, Chinese Academy of Sciences, Shanghai 201203, China. E-mail: yhhu@simm.ac.cn, hzhang@simm.ac.cn*
[b] *CAS Key Laboratory of Receptor Research, Shanghai Institute of Materia Medica, Chinese Academy of Sciences, Shanghai 201203, China*
[c] *University of Chinese Academy of Sciences, No.19A Yuquan Road, Beijing 100049, China*
[d] *School of Pharmaceutical Science and Technology, Hangzhou Institute for Advanced Study, UCAS, 1 Xiangshanzhi Road, Hangzhou, 310024, China*
[e] *School of Life Science and Technology, ShanghaiTech University, Shanghai, 201210, China*

† Electronic supplementary information (ESI) available: ThT fluorescence of Aβ incubated with QAD-1; *ex vivo* fluorescence staining of **P14**; quantitative analysis of ThS positive signals in brain sections; latency of the passage water maze test of APP/PS1 transgenic mice; synthetic details. See DOI: **https://doi.org/10.1039/d3md00744h**

‡ Jingjing Zhang and Wenming Ren contributed equally to this work.

very limited progression has been achieved in the study of AD. As mentioned above, Aβ is considered as a biomarker for both diagnosis and treatment of AD, therefore, simultaneous visualization and inhibition of Aβ at the early stage of AD have become a promising strategy for the treatment of AD.[16] In fact, a few fluorescent probes with a potential theranostic effect have been investigated in recent years. Taking together the potent inhibitory effect of curcumin on Aβ aggregation[6] and its fluorescence enhancement capability when interacting with Aβ,[17] curcumin was recognized as a potential Aβ fluorescent probe as well as a theranostic agent against the Aβ cascade. However, the *in vivo* application of curcumin was limited due to its low bioavailability and short wavelength. Since then, more studies have begun to investigate probes that could achieve *in vivo* diagnostic and therapeutic effects. Several types of curcumin derivatives were successfully discovered to possess *in vivo* diagnostic effects on Aβ plaques in the brain of AD transgenic mice; however, their therapeutic effects were restricted at either the molecular level or cellular level. Cranad-28[17] and PIB-C[18] could inhibit Aβ aggregation at the molecular level. Aggregation-induced emission (AIE) probe Cur-N-BF2 could light up upon detection of Aβ and exhibit protection of neuronal cells by inhibition of Aβ aggregation in HT-22 cells.[19] Dibutylnaphthylamine-based cyanine probe DBAN-SLM could protect SH-SY5Y cells against Aβ-induced toxicities and suppress Aβ-induced reactive oxygen species (ROS) generation.[7] As a matter of fact, the above theranostic probes still lack dual effects of diagnosis and therapy *in vivo*.

The BODIPY fluorophore is widely used to build fluorescent probes due to its excellent photophysical properties, high quantum yield, and intense absorption of visible light.[20] Watanabe *et al.* synthesized a BODIPY-based probe (BAP-2), which possessed good affinity to Aβ aggregates (Kd = 55 nM).[21] In order to increase the emission wavelength, our previous work discovered a new BODIPY-based probe, QAD-1, which exhibited a low background signal and high affinity to Aβ aggregates (Kd = 27 nM).[22] Interestingly, our recent study found that QAD-1 possesses potential therapeutic effects on Aβ aggregation using the ThT assay (Fig. S1†). Taking into consideration the above potential of the BODIPY scaffold in fluorescence imaging, we aim to develop potent theranostic agents for fluorescence imaging of cerebral Aβ and blocking the Aβ aberrant cascade.

Here, we report the synthesis, characteristics, and biological evaluations of a novel theranostic agent, **P14**, for both *in vitro* and *in vivo* imaging of central Aβ plaques, inhibition of Aβ-associated self-aggregation, and neuronal damage as well as behavioral deficits.

Experimental

Synthesis of P14

P14 was synthesized by condensation of previously reported dye **3** with aldehyde **2** (Scheme S1†) as a purple blue powder. The final product was confirmed by ^{1}H NMR, ^{13}C NMR, and high-resolution mass spectrometry and HPLC (Fig. S2–S6†).

Preparation of Aβ aggregates

The $A\beta_{42}$ monomer (0.1 mg, 1,1,1,3,3,3-hexafluoro-2-propanol (HFIP)-pretreated) was dissolved with 11 μL DMSO, followed by addition of 432 μL phosphate buffer solution (PBS, 10 mM, pH = 7.4), to a final concentration of 50 μM. Aβ aggregates were prepared by shaking the stock solution at 100 rpm for 24 h at 37 °C. The Aβ aggregates were confirmed structurally by using transmission electron microscopy.

Animals

AD transgenic mice (APP/PS1 and 5 × FAD) were obtained from the Jackson Laboratory, and the corresponding wild type (WT) control mice were littermates of the transgenic mice. Pregnant Sprague Dawley (SD) rats at 17 days of gestation were purchased from Shanghai SLAC Laboratory Animal Co., Ltd. All the animal procedures were performed in accordance with the National Institutes of Health Guide for the Care and Use of Laboratory Animals, under the protocols approved by and strictly following the guidelines of the Institutional Animal Care and Use Committee (IACUC no. 2018-08-ZHY-5 and no. 2017-02-ZHY-1).

Fluorescence spectral measurement of P14 with $A\beta_{42}$ aggregates

A solution of $A\beta_{42}$ aggregates (0, 2, 4, 6, 8 μM in the final assay mixture) was added to **P14** (final concentration: 320 nM in EtOH). The mixture solutions were incubated for 30 min at room temperature. The fluorescence emission spectra were recorded using a fluorescence spectrometer (Fluoromax-4, HORIBA). The parameters of the fluorescence spectrometer are: external slit = 10 nm, electromagnetic slit = 10 nm, PMT voltage = 700 V, excitation = 589 nm, emission = 600–800 nm.

Measurement of Kd

Ten microliters of **P14** (0–6.4 μM in EtOH) was mixed with 100 μl of $A\beta_{42}$ (10 μM in PBS) and 90 μl of PBS. The final concentrations of **P14** were 0–320 nM, the final concentration of $A\beta_{42}$ was 5 μM, and the proportion of ethanol in solution is 5%. $A\beta_{42}$ (5 μM) was added to **P14** (0 nM to 200 nM in EtOH). Samples were incubated for 30 min at room temperature, and then transferred to a quartz cuvette. The fluorescence signals were recorded using a fluorescence spectrometer (Fluoromax-4, HORIBA). The parameters of the fluorescence spectrometer are: external slit = 10 nm, electromagnetic slit = 10 nm, PMT voltage = 700 V, excitation = 589 nm, emission = 620 nm. The Kd value was calculated with PRISM software (nonlinear regression, one site-binding).

Transmission electron microscopy

1,1,1,3,3,3-Hexafluoro-2-propanol (HFIP)-pretreated $A\beta_{42}$ (0.1 mg) was dissolved in 11 μL DMSO, and then added into 432 μL H_2O to a final concentration of 50 μM. 25 μL $A\beta_{42}$ (50 μM) was mixed with an equal volume of H_2O or **P14** (100 μM), and then incubated at 37 °C shaking at 100 rpm for 24 h.

These samples were adsorbed onto carbon-film-coated copper grids (300 meshes) for 1 min and then stained with filtered 7.5% uranium formate for 1 min. The stained samples were examined and photographed on a Talos L120C transmission electron microscope (FEI) operating at 120 kV.

Fluorescence staining of brain slices from APP/PS1 transgenic mice

Frozen sections were made after perfusion and gradient dehydration of APP/PS1 mouse brains. Brain slices were incubated with ThS (10 mg mL^{-1}) as a positive control of this experiment. After 3 times washing with 50% ethanol (1 min per wash), the same slice was incubated with **P14** (100 μM) for 20 min at room temperature. After removing the residual liquid with dust free paper, the slice was then mounted with coverslips and imaged using a Leica confocal microscope (TCS SPS CFSMP).

In vivo fluorescence imaging of Aβ plaques in the brain of AD transgenic mice

The heads of AD transgenic mice and their age-matched littermates were shaved before imaging (12 months old). All animals were anaesthetized with 1.5% isoflurane supplied by a gas anesthesia system. Both transgenic and wild type mice were intravenously injected with freshly prepared **P14** solution (2 mg kg^{-1}, DMSO : Cremophor EL : 0.9% saline = 5 : 10 : 85). Fluorescence signals in the brains were acquired sequentially, and the circular regions of interest were analyzed using Living Imaging Software.

ThT fluorescence assay

ThT was dissolved in 50 mM glycine–NaOH solution and diluted to 15 mM. The $A\beta_{42}$ monomer (50 μM) was incubated with or without **P14** (100 μM) at 37 °C for 24 h. Samples were mixed with ThT in a 96-well black microplate at the total volume of 200 μL. Fluorescence intensity was measured using a microplate reader (SpectraMax M5, Molecular Devices) at 425/490 nm (excitation/emission).

Cell viability assay

The 3-(4,5-dimethylthiazol-2-yl)-2,5diphenyltetrazolium bromide (MTT) assay was conducted to evaluate cell viability. The mouse pups (postnatal 0–1) of SD pregnant rats were sterilized with 75% ethanol and then sacrificed. The brain was placed in Hanks' solution pre-cooled with an ice bag to remove the meninges and blood vessels. The cortex was cut into 1 mm pieces and digested with 0.125% trypsin. Supernatant cells were seeded in a 96-well plate at a density of 3×10^4 cells per well and cultured in neurobasal medium supplemented with B27 at 37 °C. The cells were used at 9 days and exposed to the prepared mixture of $A\beta_{42}$ (final concentration: 1 μM) and different concentrations of **P14** (final concentration: 0, 0.1, 0.25, 0.5, 1, 5 μM) for 24 h. MTT (10 μL) was added to each well and incubated for another 4 h. 100 μL dimethyl sulfoxide (DMSO) was added and the absorbance at 490 nm was recorded with a microplate reader.

Immunocytochemistry

The cells were fixed in 4% paraformaldehyde (PFA) for 10 min, followed by washing 3 times in PBS at room temperature. The cells were then blocked with 3% BSA in PBS containing 0.01% Triton X-100 for 1 h, incubated with primary antibodies overnight at 4 °C, and then washed with PBS and incubated with secondary antibodies for 1 h. The MAP2 antibody (1 : 200; Abcam; ab5392) and goat anti-mouse IgG secondary antibody, Alexa Fluor 488 (1 : 500; Invitrogen; A-11003) were used in the current study. Nuclei were stained with DAPI (1 : 5000; Sigma).

Passage water maze test

The passage water maze (80 cm × 50 cm) contains only one correct path to the platform in the passage maze, and the rest are interference paths. The experimental task includes a training phase and a testing phase. During the training phase, mice were placed in a passage water maze and allowed to swim freely for 1 min. After climbing up the escape platform, the mice were wiped with a dry towel and placed in their home cage. If the mice failed to reach the target platform within 1 min, they were guided along the correct path to the platform and removed. During the testing phase, the mice were allowed to find the platform freely, and the latency to find the target platform and the number of wrong paths were recorded after training 4 times.

P14 chronic treatment in AD transgenic mice

Five month old 5 × FAD transgenic mice and wild-type mice were administered with **P14** (10 mg kg^{-1}, PEG400 : HS15 : 0.9% saline = 25 : 15 : 60) or a vehicle (PEG400 : HS15 : 0.9% saline = 25 : 15 : 60) orally for one month.

Nine month old APP/PS1 transgenic mice and wild-type mice were administered with **P14** (10 mg kg^{-1}, PEG400 : HS15 : 0.9% saline = 25 : 15 : 60) or a vehicle (PEG400 : HS15 : 0.9% saline = 25 : 15 : 60) orally for three months.

Statistical analysis

Data were shown as mean ± standard deviation. The significant differences between the two groups were analyzed by Student's *t*-test. One-way ANOVA combined with the Dunnett post-test was used among multiple groups. Two-way ANOVA was used to evaluate significant interaction between the two factors, time and genotype. $P < 0.05$ was used as the criterion to indicate a statistically significant difference.

Results and discussion

Probe design

The BODIPY scaffold was widely used in the discovery of fluorescent probes for bioimaging, including Aβ imaging. In previous study, the fluorescent probe BAP-2 which was

substituted by styryl at the α-position showed high affinity for Aβ aggregates *in vitro* and could rapidly cross the blood–brain barrier (BBB). However, its application in *in vivo* Aβ imaging failed due to the rapid accumulation in the scalp and the strong noise fluorescence induced by accumulation.[21] Herein, we designed a strategy to introduce a flexible alkyl chain possessing a hydrophilic hydroxyl to the BODIPY core to reduce the accumulation. We also replaced the thiophene with thiazole to synthesize the final fluorescent probe **P14**, which possessed higher solubility in H_2O (Fig. 1). *In vitro* and *in vivo* studies were further carried out to investigate the theranostic effect of **P14** against the Aβ cascade.

Fluorescence responses of P14 to Aβ aggregates

To evaluate the affinity of **P14** with Aβ comprehensively, *in vitro* and *in vivo* experiments were both conducted. The Kd constant was estimated by conducting fluorescence titrations. As shown in Fig. 2A, **P14** displays a high binding affinity toward Aβ aggregates (Kd = 78.08 nM). The fluorescence enhancement of **P14** incubated with $Aβ_{42}$ aggregates was further measured. As shown in Fig. 2B, when different concentrations of $Aβ_{42}$ aggregates (final concentration: 0 μM, 2 μM, 4 μM, 6 μM and 8 μM) were added to **P14** (final concentration: 320 nM) solution, the fluorescence intensity of probe **P14** increased significantly. These results show that **P14** has a good response to Aβ aggregates at the molecular level.

The ability of **P14** to stain Aβ plaques was tested in brain slices from double transgenic mice (APPswe/PSEN1dE9, APP/PS1, 12 months old, male), which were widely used in Aβ fluorescence imaging.[22,23] The result showed that there were high contrast fluorescent spots (red) in the cerebral cortex and hippocampus (Fig. 2C) of APP/PS1 transgenic mice, which were confirmed to be Aβ plaques as the red fluorescent spots could well co-localize with ThS-stained signals (green). By contrast, no noticeable signals were observed in **P14**-incubated brain sections from age-matched wild-type mice. Our results indicated that **P14** could fluorescently label Aβ plaques with a low background signal *in vitro*.

In vivo fluorescence imaging of P14 in AD transgenic mice

With the favorable *in vitro* Aβ binding properties and good lipophilicity of **P14**, *in vivo* Aβ imaging was performed on APP/PS1 transgenic mice with their age-matched wild-type mice (C57BL6) used as the control. An IVIS Spectrum imaging system (PerkinElmer) was used to assess the *in vivo* fluorescence imaging ability of **P14** for Aβ plaques in the brain of APP/PS1 transgenic mice. After intravenous injection of **P14** at 2.0 mg kg^{-1} dosage, the images of the brain of APP/PS1 or wild type mice were recorded using the IVIS spectral imaging system (Perkin/Elmer). As shown in Fig. 3, the fluorescence intensity of transgenic mice was significantly higher than that of wild type mice at the time of 5 minutes after **P14** injection. Statistically significant differences in fluorescence signals could be attributed to the high fluorescence enhancement and binding affinity of **P14** towards Aβ. The *in vivo* result was further confirmed by *ex vivo* histology (Fig. S7†). These results indicated that **P14** had the capacity for labeling central Aβ *in vivo*.

In vitro effects of P14 against Aβ-associated neuronal damage

As the underlying mechanism of the active compound for triggering fluorescence response upon Aβ aggregation or inhibiting Aβ aggregation could be attributed to the interaction between the compound and Aβ, therefore the afore-mentioned Aβ labeling effect of **P14** suggests its potent interaction with Aβ and might indicate its potential therapeutic effect against Aβ-associated abnormalities. First of all, we tested the inhibitory effect of **P14** on Aβ aggregation *in vitro*. The aggregation states of $Aβ_{42}$ were identified by the ThT fluorescence assay. **P14** was incubated with $Aβ_{42}$ for 24 h (37 °C), and the inhibition rate on ThT fluorescence was measured. As shown in Fig. 4A, the **P14** (0.1–5 μM) concentration dependently inhibited the ThT-induced enhancement of fluorescence signals when incubated with aggregated $Aβ_{42}$. Moreover, morphological changes of Aβ aggregate states after incubation with **P14** were observed by transmission electron microscopy (TEM). As shown in Fig. 4B, $Aβ_{42}$ was found to form amyloid fibrils

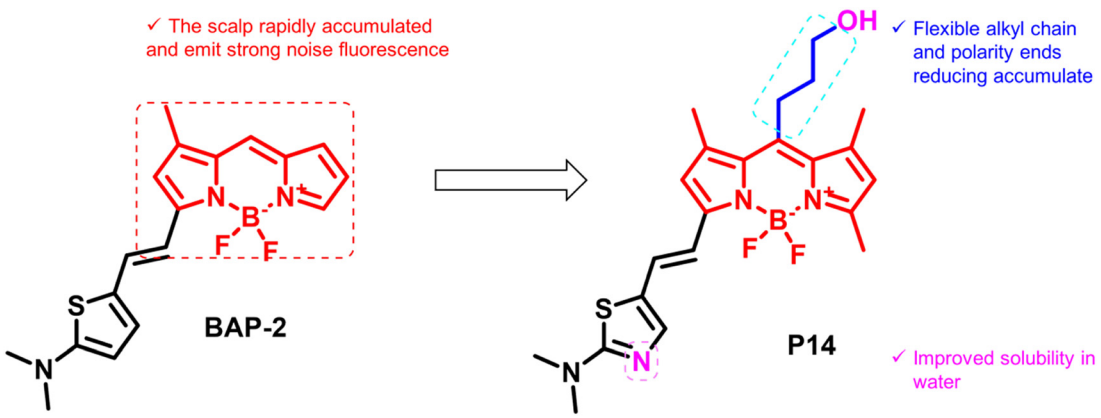

Fig. 1 Probe design strategy of **P14**.

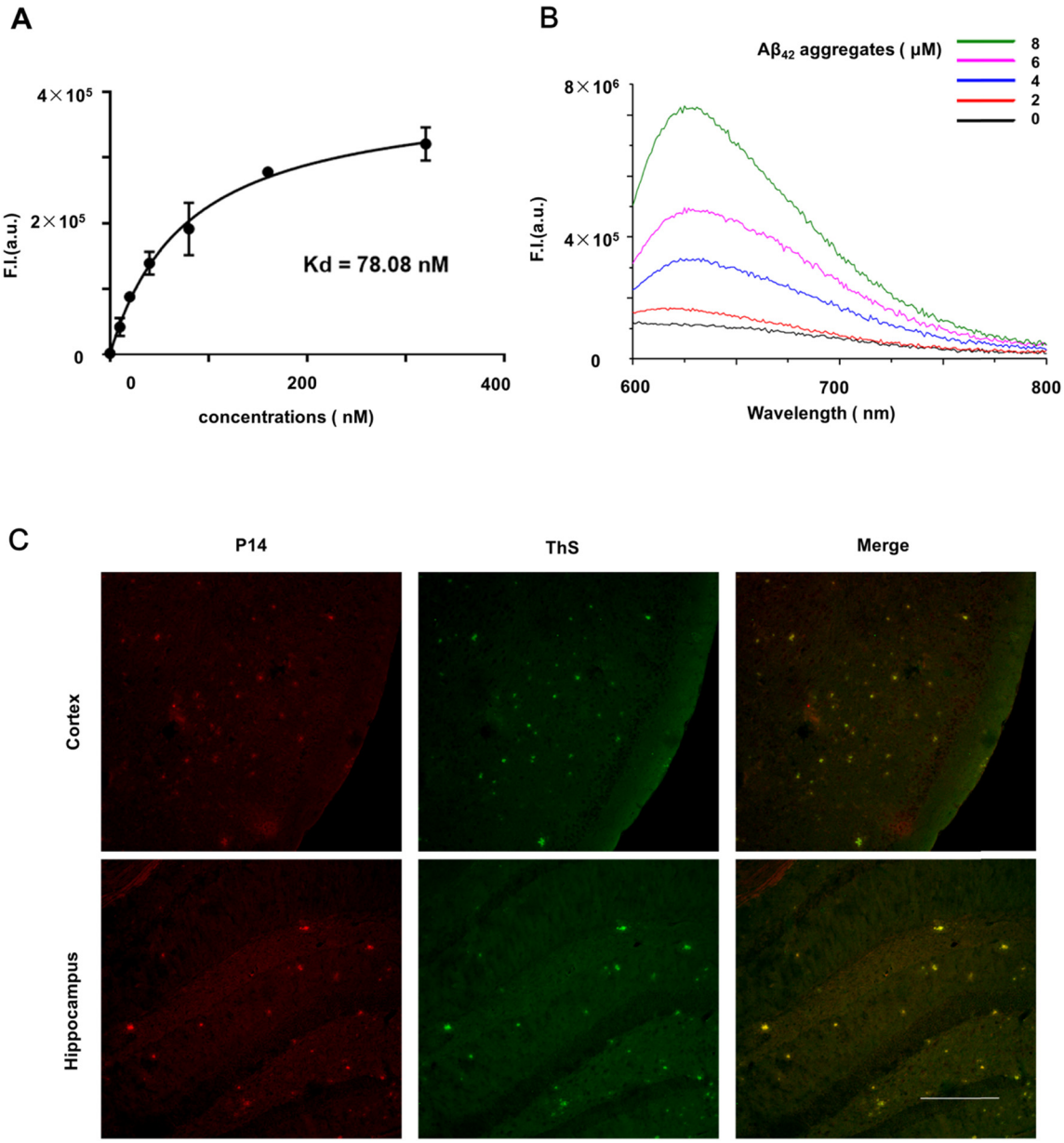

Fig. 2 (A) Kd of **P14** to $A\beta_{42}$ aggregates (Ex = 589 nm, Em = 620 nm); (B) fluorescence responses of **P14** (1 μM) with different concentrations of $A\beta_{42}$ aggregates (Ex = 589 nm; Em = 600–800 nm); (C) fluorescence staining of Aβ deposits with **P14** and ThS in the cortex and hippocampus of 12 month-old APP/PS1 mice (n = 3). The excitation channel for **P14** imaging = 638 nm, emission channel = 650–700 nm; the excitation channel for ThS imaging = 488 nm, emission channel = 500–550 nm; scale bar = 250 μm; data are presented as the mean ± SD, n = 3.

after incubation for 24 h. By contrast, incubation of Aβ with **P14** was observed with reduced density of amyloid fibrils, indicating that **P14** could inhibit the aggregation of Aβ.

Considerable evidence indicated that Aβ aggregates caused various functional impairments on neurons including neuronal damage and synaptic loss.[24] Therefore, cellular experiments were carried out to further assess the protective effects of **P14** against $A\beta_{42}$-induced neuronal injuries. Primary cortical neurons were incubated with the $A\beta_{42}$ monomer (1 μM) and different concentrations of **P14** (0, 0.1, 0.25, 0.5, 1, 5 μM) at 37 °C for 24 h. As shown in Fig. 5A, **P14** at 1 μM and 5 μM significantly ameliorated $A\beta_{42}$-induced reduction in the cell viabilities of primary cortical neurons. Moreover, the influence of **P14** on $A\beta_{42}$-induced synaptic deficits was further assessed by staining of MAP2 (microtubule-associated protein 2), a cytoskeleton protein expressed in neurons, which is an important protein marker of dendrites and widely used to assess synaptic changes.[25] Results showed that MAP2 signals of primary cortical neurons were significantly reduced by $A\beta_{42}$ exposure, while **P14** (1 μM) incubation alleviated $A\beta_{42}$-induced loss of MAP2 signals in primary cortical neurons (Fig. 5B). The statistical results showed that the ratio of the MAP2/DAPI fluorescence signal of the $A\beta_{42}$ model group

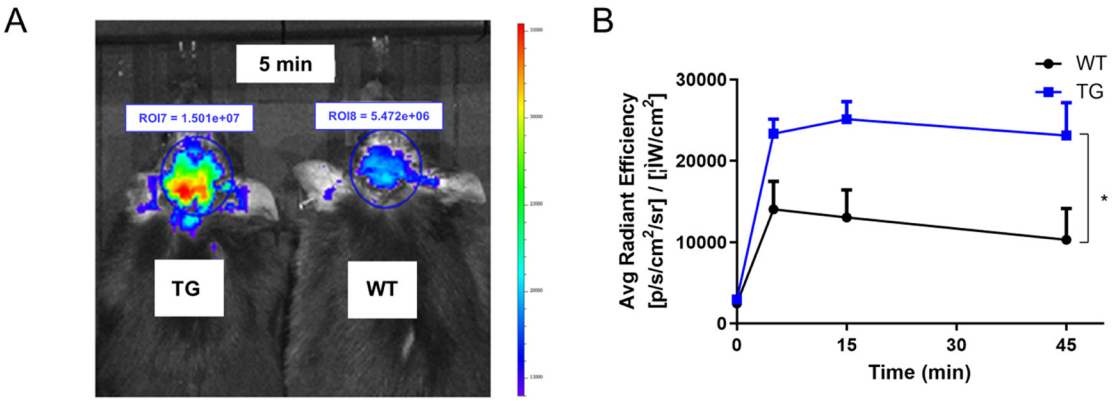

Fig. 3 (A) Representative IVIS images of the brain of 12 month old APP/PS1 and wild-type mice. (B) Statistical results of the fluorescence signal intensity of the brains. Ex = 570 nm, Em = Cy5.5. Data are presented as the mean ± SD, n = 3, $^{*}P < 0.05$, compared with the WT group. WT: wild type mice; TG: APP/PS1 mice.

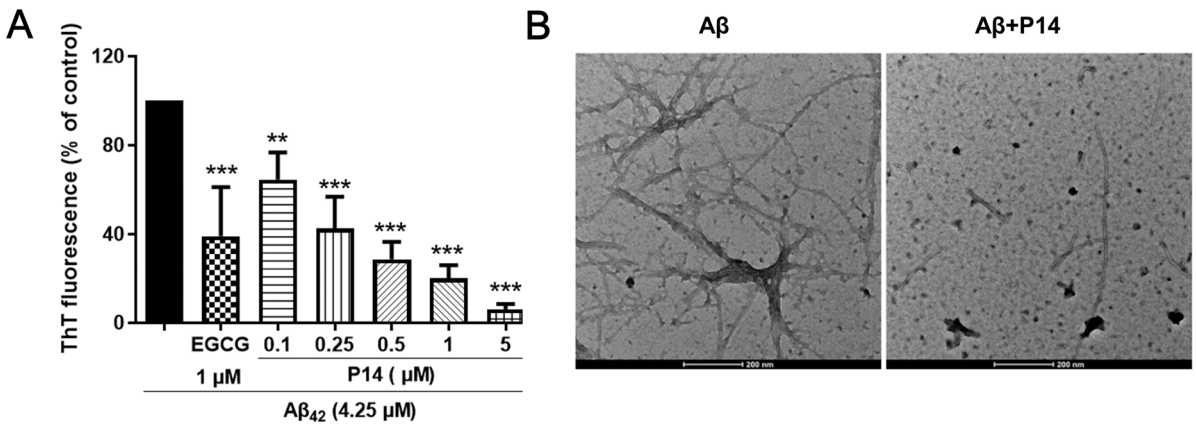

Fig. 4 (A) ThT fluorescence of Aβ incubated with different concentrations of **P14**. Data are presented as the mean ± SD, n = 4, $^{**}P < 0.01$, $^{***}P < 0.001$ compared with the $A\beta_{42}$ alone group. (B) Representative transmission electron microscopy (TEM) images of $A\beta_{42}$ aggregates or $A\beta_{42}$ incubated with **P14** (50 μM) (24 h) (scale bar = 200 nm).

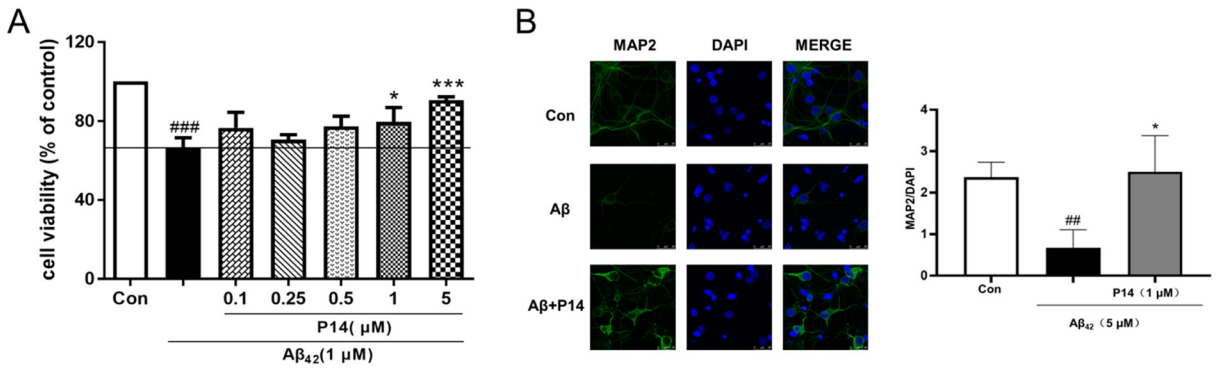

Fig. 5 (A) Cell viability conducted by the MTT assay. (B) Representative immunofluorescence staining of MAP2 in primary neurons. Statistical results of immunofluorescence staining of MAP2 in primary neurons. Data are presented as the mean ± SD, n = 3; $^{\#\#}P < 0.01$, $^{\#\#\#}P < 0.001$ compared with the control group; $^{*}P < 0.05$, $^{***}P < 0.001$ compared with the Aβ group. Con: control group.

was significantly lower than that of the control group ($P < 0.01$), while **P14** treatment significantly reversed the reduction of MAP2 fluorescence signals induced by $A\beta_{42}$ exposure ($P < 0.05$ *vs.* $A\beta_{42}$ group) (Fig. 5B). By contrast, **P14** alone at 0.1 to 5 μM concentrations had no obvious influence on the cell viabilities of primary neurons (Fig. S8†). The above results suggested that **P14** could alleviate $A\beta_{42}$-associated neuronal injuries.

In vivo effects of P14 against Aβ-associated cognitive impairment

To explore the therapeutic effect of **P14** against Aβ-associated disorders *in vivo*, two classic AD transgenic mice models—APP/PS1 transgenic mice and 5 × FAD mice—were used. APPswe/PSEN1dE9 (APP/PS1) mice carried two transgenes with AD-linked mutations: a chimeric mouse/human APP with the Swedish mutation and human PSEN1 lacking exon 9 (dE9).[26] 5 × FAD mice carried three mutations of the human amyloid precursor gene (Swedish K670N/M671L, Florida-I716V, and London-V717I) and two mutations of the human presenilin-1 gene (M146L and L286V).[27] Aβ plaques in the brain of 5 × FAD transgenic mice were measured after one-month administration of **P14**. Immunofluorescence staining results showed that the number of Aβ plaques in both the hippocampus and cortex of APP/PS1 mice was decreased significantly after 3 month administration of **P14** (Fig. 6A and S9A†), as compared to that of vehicle-administered transgenic mice. Similarly, the number of Aβ plaques in the hippocampus of **P14**-treated 5 × FAD transgenic mice decreased significantly compared with that of the vehicle-treated 5 × FAD transgenic animal group (Fig. 6B and S9B†). The above results from the two types of AD transgenic mice indicate that **P14** could inhibit Aβ aggregation *in vivo*.

APP/PS1 transgenic mice were further used to evaluate the ameliorative effect of **P14** on cognitive impairment, by assessing their behavioural performance in a passage water maze, which could evaluate the ability of rodents to memorize complex paths.[28] After 3 months of administration (9 months to 12 months) with **P14**, the error times ($p < 0.01$) of APP/PS1 mice in the passage water maze were significantly enhanced, as compared to those of wild type (WT) mice. By contrast, the error times of **P14**-treated APP/PS1 transgenic mice were significantly reduced ($p < 0.05$ *vs.* TG mice) (Fig. 6C). Similarly, the latencies of reaching the platform were shortened compared to those of TG mice ($p = 0.1230$) (Fig. S10†). These results suggest that **P14** could ameliorate cognitive impairment in AD transgenic mice.

Application of P14 for disease and therapy monitoring

Monitoring the central Aβ cascade during disease progression and after treatment with effective therapeutics could provide real-time knowledge of the internal disease state, which could also provide important clues for the efficient discovery of potential drugs against AD.[29] Recently, Ran's group reported a curcumin analogue CRANAD-3,[23] which was used for monitoring short-term and chronic treatments. Based on the aforementioned results of **P14** in Aβ visualization and inhibition, one month administration of **P14** along with fluorescence imaging was conducted in 5 × FAD transgenic mice. Fluorescence intensities of 5 month 5 × FAD transgenic mice and wild type mice were recorded after single intravenous injection of **P14** (2.0 mg kg^{-1}). Results showed that the average radiation efficiency (ARE) of 5 × FAD transgenic mice was significantly higher than that of WT mice. The peak ARE of TG mice was 6.7e + 008 P S^{-1} cm^{-2} Sr^{-1} μW^{-1} cm^{-2} (Fig. 7A and B). After 1 month of administration with **P14** (p.o., 30 mg kg^{-1}), the ARE of **P14**-treated 5 × FAD transgenic mice was significantly lower than that of vehicle-treated 5 × FAD transgenic mice ($P < 0.05$). The peak ARE of the **P14** treatment group was 5.2e + 008 P S^{-1} cm^{-2} Sr^{-1} μW^{-1} cm^{-2} (Fig. 7C and D). The result indicated that **P14** administration could reduce the central Aβ aggregation *in vivo* in AD transgenic mice. In addition, the peak ARE of the 6 month-old 5 × FAD transgenic mice was 7.7e + 008 P S^{-1} cm^{-2} Sr^{-1} μW^{-1} cm^{-2}, higher than that of the 5 × FAD transgenic mice at 5 months old (Fig. 7). Taken together, the above results suggested that **P14** possessed

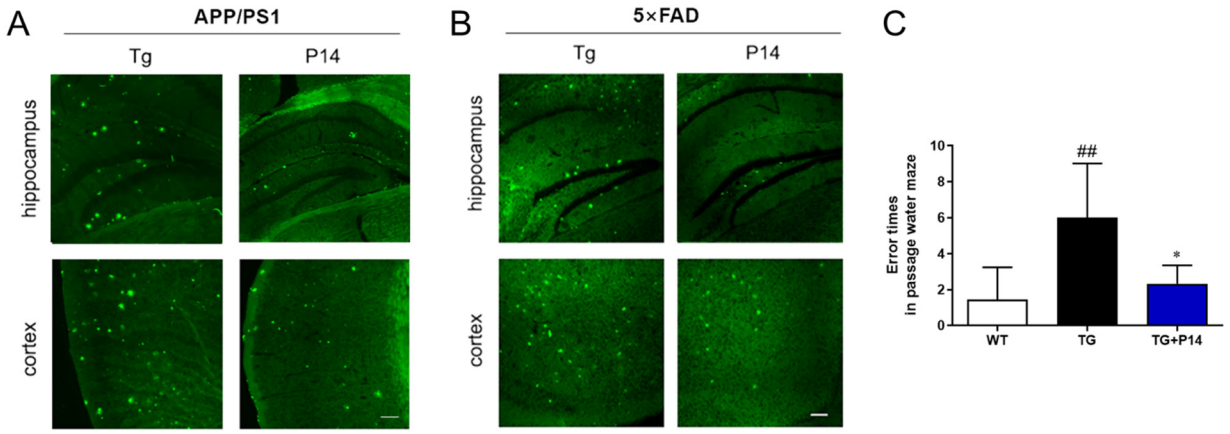

Fig. 6 (A) Representative confocal images of ThS staining (green) in the hippocampus and cortex from 12 month-old APP/PS1 transgenic mice after administering **P14** continuously for 3 months ($n = 3$); scale bar = 100 μm. (B) Representative confocal images of ThS staining (green) in the hippocampus and cortex from 6 month-old 5 × FAD mice after administering **P14** continuously for 1 month ($n = 9$–10); scale bar = 100 μm. (C) Error times of the passage water maze test of 12 month-old APP/PS1 transgenic mice and their littermates after administering **P14** or a vehicle continuously for 3 months. Data are presented as the mean ± SD, $^{\#\#}P < 0.01$ compared with the WT group; $^{*}P < 0.05$, compared with the TG group; $n = 6$–10. WT: wild type mice; TG: APP/PS1 mice.

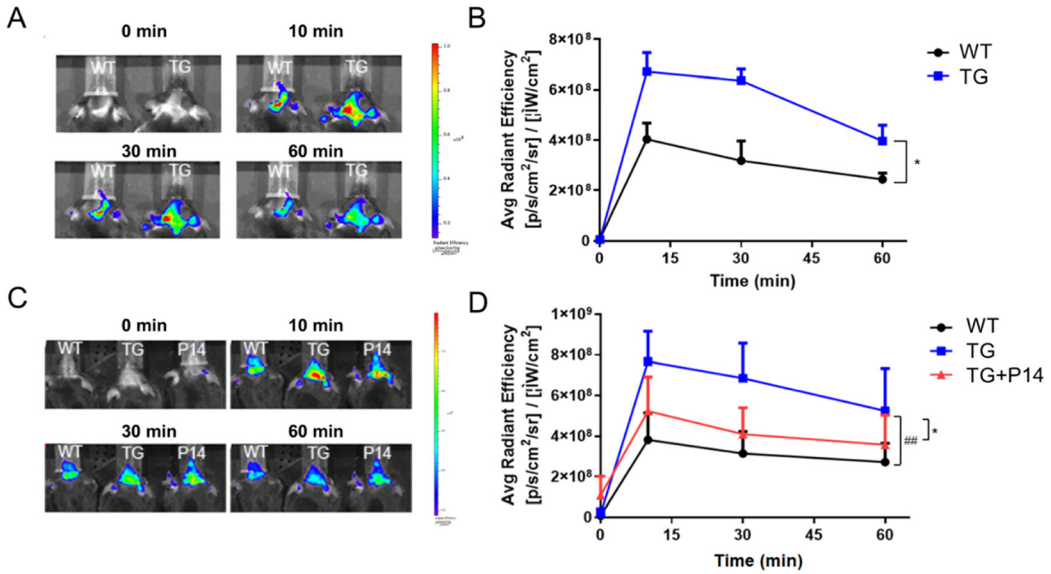

Fig. 7 (A) Representative Aβ imaging pictures of 5 month-old 5 × FAD transgenic (TG) mice or wild type (WT) mice. (B) Quantitative analysis results of *in vivo* Aβ imaging in A (n = 3). (C) Representative imaging pictures of 6 month-old TG mice or WT mice with one month administration of **P14** or a vehicle. (D) Quantitative analysis results of *in vivo* Aβ imaging in C (n = 4). Aβ imaging was conducted after intravenous injection of **P14**. Ex = 570 nm, Em = 640 nm. Data are presented as the mean ± SD. WT: wild type mice; TG: 5 × FAD mice.

theranostic potential against the Aβ cascade in AD transgenic mice.

Conclusions

In summary, a potential theranostic probe **P14** was discovered to target Aβ, which was believed to be both a biomarker and key pathological protein in the progress of AD. **P14** is the first BODIPY skeleton-based theranostic probe for Aβ and showed good characteristics of a fluorescent probe including high sensitivity, significant fluorescence enhancement towards Aβ, and the ability to rapidly cross the BBB. **P14** also inhibits Aβ self-aggregation and ameliorates Aβ-associated neuronal damage and behavioral deficits in AD transgenic animals. Moreover, **P14** was successfully applied to monitor the progression of Aβ aggregation and the therapeutic effect itself in the brain of 5 × FAD transgenic mice by fluorescence imaging. These results indicate that **P14** is a novel BODIPY-based theranostic agent that can be used *in vivo*, and provides important clues for the discovery of good fluorescent probes for monitoring the Aβ progression.

Author contributions

Jingjing Zhang: conceptualization; investigation; methodology; writing – original draft; funding acquisition. Wenming Ren: conceptualization; investigation; methodology. Jingjing Chen: methodology; writing – original draft. Xiaohui Liu/Yuteng Zeng/Huaijiang Xiang: formal analysis. Youhong Hu/Haiyan Zhang: conceptualization; supervision; writing – review and editing; funding acquisition.

Conflicts of interest

There are no conflicts to declare.

Acknowledgements

The authors acknowledge the financial support through the funds from the National Science and Technology Innovation 2030 Major Program (Grant No. 2021ZD0200900), the National Natural Science Foundation of China (Grant No. 82003724), the China Postdoctoral Science Foundation Grant (Grant No. 2019M661669), the National S&T Major Projects (Grant No. 2018ZX09711002) and the Shanghai Municipal Science and Technology Major Project (Grant No. 2018SHZDZXO5).

Notes and references

1 F. Panza, M. Lozupone, G. Logroscino and B. P. Imbimbo, *Nat. Rev. Neurol.*, 2019, **15**, 73–88.
2 L. Apostolova, *J. Clin. Psychiatry*, 2021, **82**(3), BG20044WC1C.
3 R. A. Sperling, P. S. Aisen, L. A. Beckett, D. A. Bennett, S. Craft, A. M. Fagan, T. Iwatsubo, C. R. Jack, Jr., J. Kaye, T. J. Montine, D. C. Park, E. M. Reiman, C. C. Rowe, E. Siemers, Y. Stern, K. Yaffe, M. C. Carrillo, B. Thies, M. Morrison-Bogorad, M. V. Wagster and C. H. Phelps, *Alzheimer's Dementia*, 2011, **7**, 280–292.
4 S. A. Kent, T. L. Spires-Jones and C. S. Durrant, *Acta Neuropathol.*, 2020, **140**, 417–447.
5 V. Ntziachristos, C. Bremer and R. Weissleder, *Eur. Radiol.*, 2003, **13**, 195–208.
6 U. Shabbir, M. Rubab, A. Tyagi and D. H. Oh, *Int. J. Mol. Sci.*, 2020, **22**(1), 196.

7 X. Wang, C. Wang, H. N. Chan, I. Ashok, S. K. Krishnamoorthi, M. Li, H. W. Li and M. S. Wong, *Talanta*, 2021, **224**, 121830.
8 J. Yang, F. Zeng, Y. Ge, K. Peng, X. Li, Y. Li and Y. Xu, *Bioconjugate Chem.*, 2020, **31**, 2–15.
9 H. Wang, J. Zhang, F. Dou and Z. Chen, *Biosens. Bioelectron.*, 2020, **153**, 112048.
10 H. Y. Yang, J. J. Zhang, Y. Zang, H. Y. Zhang, J. Li, G. R. Chen and X. P. He, *Dyes Pigm.*, 2017, **136**, 224–228.
11 R. R. Tao, N. Wang, T. R. Shen, Y. H. Tan, Y. Ren, W. J. Wei, M. H. Liao, D. Tan, C. Z. Tang, N. G. Xu, H. Wang, X. G. Liu and X. Li, *Theranostics*, 2022, **12**, 2549–2559.
12 M. P. McNerney, K. E. Doiron, T. L. Ng, T. Z. Chang and P. A. Silver, *Nat. Rev. Genet.*, 2021, **22**, 730–746.
13 S. Jeyamogan, N. A. Khan and R. Siddiqui, *Arch. Med. Res.*, 2021, **52**, 131–142.
14 M. E. Lobatto, V. Fuster, Z. A. Fayad and W. J. Mulder, *Nat. Rev. Drug Discovery*, 2011, **10**, 835–852.
15 P. Ramos-Cabrer, F. Campos, T. Sobrino and J. Castillo, *Stroke*, 2011, **42**, S7–S11.
16 M. Staderini, S. Aulic, M. Bartolini, H. N. Tran, V. Gonzalez-Ruiz, D. I. Perez, N. Cabezas, A. Martinez, M. A. Martin, V. Andrisano, G. Legname, J. C. Menendez and M. L. Bolognesi, *ACS Med. Chem. Lett.*, 2013, **4**, 225–229.
17 X. Zhang, Y. Tian, P. Yuan, Y. Li, M. A. Yaseen, J. Grutzendler, A. Moore and C. Ran, *Chem. Commun.*, 2014, **50**, 11550–11553.
18 Y. Tian, X. Zhang, Y. Li, T. M. Shoup, X. Teng, D. R. Elmaleh, A. Moore and C. Ran, *Chem. Commun.*, 2014, **50**, 15792–15795.
19 Y. Yang, S. Li, Q. Zhang, Y. Kuang, A. Qin, M. Gao, F. Li and B. Z. Tang, *J. Mater. Chem. B*, 2019, **7**, 2434–2441.
20 F. F. Wang, Y. J. Liu, B. B. Wang, L. X. Gao, F. L. Jiang and Y. Liu, *Dyes Pigm.*, 2018, **152**, 29–35.
21 H. Watanabe, M. Ono, K. Matsumura, M. Yoshimura, H. Kimura and H. Saji, *Mol. Imaging*, 2013, **12**, 338–347.
22 W. Ren, J. Zhang, C. Peng, H. Xiang, J. Chen, C. Peng, W. Zhu, R. Huang, H. Zhang and Y. Hu, *Bioconjugate Chem.*, 2018, **29**, 3459–3466.
23 X. L. Zhang, Y. L. Tian, C. Zhang, X. Y. Tian, A. W. Ross, R. D. Moir, H. B. Sun, R. E. Tanzi, A. Moore and C. Z. Ran, *Proc. Natl. Acad. Sci. U. S. A.*, 2015, **112**, 9734–9739.
24 M. Talantova, S. Sanz-Blasco, X. Zhang, P. Xia, M. W. Akhtar, S. Okamoto, G. Dziewczapolski, T. Nakamura, G. Cao, A. E. Pratt, Y. J. Kang, S. Tu, E. Molokanova, S. R. McKercher, S. A. Hires, H. Sason, D. G. Stouffer, M. W. Buczynski, J. P. Solomon, S. Michael, E. T. Powers, J. W. Kelly, A. Roberts, G. Tong, T. Fang-Newmeyer, J. Parker, E. A. Holland, D. Zhang, N. Nakanishi, H. S. Chen, H. Wolosker, Y. Wang, L. H. Parsons, R. Ambasudhan, E. Masliah, S. F. Heinemann, J. C. Pina-Crespo and S. A. Lipton, *Proc. Natl. Acad. Sci. U. S. A.*, 2013, **110**, E2518–E2527.
25 J. Chen, Y. Kanai, N. J. Cowan and N. Hirokawa, *Nature*, 1992, **360**, 674–677.
26 R. Minkeviciene, J. Ihalainen, T. Malm, O. Matilainen, V. Keksa-Goldsteine, G. Goldsteins, H. Iivonen, N. Leguit, J. Glennon, J. Koistinaho, P. Banerjee and H. Tanila, *J. Neurochem.*, 2008, **105**, 584–594.
27 H. Oakley, S. L. Cole, S. Logan, E. Maus, P. Shao, J. Craft, A. Guillozet-Bongaarts, M. Ohno, J. Disterhoft, L. Van Eldik, R. Berry and R. Vassar, *J. Neurosci.*, 2006, **26**, 10129–10140.
28 R. Wang, Y. Tang, B. Feng, C. Ye, L. Fang, L. Zhang and L. Li, *Neuroscience*, 2007, **149**, 739–746.
29 H. J. Yang, F. T. Zeng, Y. C. Luo, C. Zheng, C. Z. Ran and J. Yang, *Molecules*, 2022, **27**, 3879.